

Article

The Influence of Holding Time on the Microstructure Evolution of Mg–10Zn–6.8Gd–4Y Alloy during Semi-Solid Isothermal Heat Treatment

Shuang Nie ¹, Bingyang Gao ¹, Xuejian Wang ¹, Zhiqiang Cao ^{1,*}, Enyu Guo ^{1,*} and Tongmin Wang ^{1,2}

¹ Key Laboratory of Solidification Control and Digital Preparation Technology (Liaoning Province), School of Materials Science and Engineering, Dalian University of Technology, Dalian 116024, China; nieshuang30@163.com (S.N.); gby_dlut@163.com (B.G.); wangxuejian0618@163.com (X.W.); tmwang@dlut.edu.cn (T.W.)

² Key Laboratory of Materials Modification by Laser, Ion, and Electron Beams (Ministry of Education), School of Materials Science and Engineering, Dalian University of Technology, Dalian 116024, China

* Correspondence: caozq@dlut.edu.cn (Z.C.); eyguo@dlut.edu.cn (E.G.); Tel.: +86-411-8470-6169 (Z.C.); +86-411-8470-9500 (E.G.)

Received: 11 March 2019; Accepted: 3 April 2019; Published: 8 April 2019



Abstract: A semi-solid microstructure of Mg–10Zn–6.8Gd–4Y alloys is acquired via an isothermal heat treatment process, and the effects of the holding time on the microstructure evolution of Mg–10Zn–6.8Gd–4Y alloys are investigated. The results show that the microstructure of the cast alloy is composed of primary α -Mg dendritic grains with a eutectic structure (W-phase and eutectic Mg) distributed at the grain boundaries. The primary α -Mg dendritic grains grow in size with increasing holding time, and they tend to grow into more globular structures in the initial stage; they then become a bit more dendritic, as small branches grow from the grain boundaries after holding the sample at 580 °C for 10 min. Meanwhile, the interdiffusion of magnesium atoms within the eutectic region, and between the primary α -Mg and eutectic structure, leads to the formation of fine and relatively globular eutectic Mg grains in the eutectic structure after holding for 10 min. The eutectic Mg grains begin to grow, coarsen, coalesce, or be swallowed by the surrounding primary grains, causing fluctuations of the general grain size. Over the whole isothermal heat treatment process, two mechanisms—coalescence and Ostwald ripening—dominate the grain coarsening.

Keywords: magnesium alloy; semi-solid; isothermal coarsening; microstructure evolution

1. Introduction

Magnesium alloys have become important structural material candidates for applications in the automotive and aerospace industries alongside other fields due to their high specific strength and stiffness, as well as the simplicity of processing them to fabricate products [1]. Adding rare-earth (RE) elements has been proven to be a feasible and effective method to strengthen magnesium alloys [2–4]. Owing to the unique properties of rare-earth (RE) elements, their addition can significantly improve the performance of magnesium alloys [5]. The solid solubility of gadolinium (Gd) in magnesium can reach 24 wt.%, and this will lead to solid solution strengthening [4,6]. In addition, a eutectic phase with Mg can be formed after adding Gd, which reinforces the heat resistance of the alloys [7]. Yttrium has similar characteristics to Gd. It allows strengthening of magnesium by precipitation strengthening and solid solution strengthening [2]. However, casting defects limit the addition of RE elements into magnesium alloys and consequently restrict the application and development of rare-earth elements in magnesium alloys [8].

To make full use of these scarce and valuable resources, it is important to consider the manufacturing process for Mg–RE alloys. Semi-solid metal forming (SSMF), proposed by Flemings [9], is considered to be a promising method. Magnesium alloys produced by the SSMF process have lower porosity, longer die life, and lower tendency towards hot tearing, when compared with the ones made by conventional casting [10,11]. Currently, magnesium alloys used in SSMF processing are mainly confined to commercial Mg–Al alloys, including AM50, AZ91, and AM60 [12,13]. Isothermal heat treatment of alloys in the semi-solid temperature range was discovered to be an economically efficient technique to generate globular structures for their subsequent formation [14]. During the isothermal treatment process, the initial dendritic structures would grow and coarsen to be spherical, and the morphology of the secondary phase would be modified during the holding time of the process [15–17]. Ostwald ripening and coalescence mechanisms have important impacts on microstructure evolution and control the grain coarsening over the whole process. Ostwald ripening involves the diffusion of solute atoms from small grains to the larger ones. The driving force for the diffusion flow between grains is well-understood to be the chemical potential difference between the grains and domain surfaces, which generally requires the chemical potential of the curved interface to be different from that of the flat one [18]. The diffusion process causes the large structures to grow and coarsen, and the smaller structures decrease in size or even dissolve. The prerequisite for coalescence is that the sizes of two adjacent grains are different, so that the larger grains absorb the smaller ones when the grain boundary is dissolving. Likewise, if there is a low crystallographic disorientation between the adjacent grains, this can also trigger coalescence [19,20]. The systems that have high values of the solid–liquid interfacial energy coarsen by Ostwald ripening. On the contrary, the grains tend to coalesce when the volume fraction of grains is low and especially when the interfacial energy is very low.

Owing to the importance of coarsening, many studies have been undertaken to investigate the coarsening process during solidification or under isothermal heat treatment in metallic alloy systems [21–24]. Some of the coarsening mechanisms are revealed in those studies through examining the 2D microstructures. However, the samples' microstructures are likely to be destroyed during sample preparation, such as during cutting, polishing, and etching, and thus may not reflect the real microstructures in three-dimensional (3D) space. This can now be improved by the use of synchrotron tomography (SR-CT) to nondestructively characterize the 3D microstructure or even 4D (3D + time) structure of metallic materials [25–30]. For example, to explore the dynamics of microstructure evolution during coarsening, some work on Mg–Zn alloys has been performed by Guo et al. using 4D synchrotron tomography [29].

In this work, the microstructure evolution of Mg–10Zn–6.8Gd–4Y alloy during isothermal heat treatment is investigated. For this purpose, the alloy is initially solidified, then heated up to a semi-solid temperature, and held for various amounts of time before the sample is quenched for post-study examination. The structure of this alloy is analyzed by scanning electron microscope (SEM), synchrotron X-ray tomography, and electron probe microscope analysis (EPMA). The dendritic microstructural evolution of the alloy in the semi-solid state at the temperature of processing is explored. The mechanism controlling the microstructure evolution is the focus of this paper and is discussed.

2. Materials and Methods

The studied material in this paper was cast Mg–10Zn–6.8Gd–4Y (all in wt.%) alloy which was prepared by adding the following materials: high-purity elemental Mg (>99.99%) and Zn (>99.99%), Mg–30wt.%Gd, and Mg–30wt.%Y master alloys. The materials were melted in a MgO crucible electric resistance furnace under a protective atmosphere of SF₆ (1 vol.%) and CO₂ (bal.) and cast into a cylindrical steel mold (Φ 80 × 100 mm). The actual chemical composition, as determined quantitatively by inductively coupled plasma atomic emission spectroscopy (ICP-AES), was 79.2wt.%Mg–9.97wt.%Zn–6.78 wt.%Gd–4.05wt.%Y. Subsequently, the ingot was machined into the Φ 1 × 30 mm³ samples for the isothermal heat treatment experiments that were performed in a tubular

vacuum furnace. The specimens were reheated to 580 °C and isothermally held for 2.5, 5, 10, 15, 30, 60, and 120 min. Subsequently, the samples were quenched into cold water at room temperature.

Small samples were machined and prepared by the standard metallography procedure. After etching with 4 vol.% nitric acid in ethanol, the phase identification was performed by an X-ray diffractometer (XRD, EMPYREAN, Malvern Panalytical, Eindhoven, The Netherlands), using Cu K α radiation. The microstructure was characterized with an SEM (Zeiss Supra 55, Oberkochen, Germany) equipped with an energy-dispersive spectrometer (EDS) and an EPMA (JXA-8530F Plus, Tokyo, Japan) operated at 15 kV and 1×10^{-8} A. The composition and crystal structure of the eutectic phase were detected by transmission electron microscopy (TEM, JEOL JEM-2100F, Tokyo, Japan) operated at 200 kV. The microstructure characteristics, such as the average grain size, were analyzed quantitatively using the software ImageJ (National Institutes of Health, Maryland, the United States). The grains in the SEM images were separated by ImageJ, and then the number of grains in each image was counted, and finally, the average grain size was calculated.

The tomography experiments were conducted at the BL13W1 beamline of the Shanghai Synchrotron Radiation Facility (SSRF). For the tomography, a transmitted beam of 25 keV was used to penetrate the Φ 1 mm sample. The projections were recorded by a high-speed charge coupled device (CCD) camera. The distance between the specimen and camera was \sim 20 cm. During each scan, 1080 projections were collected over a 180° rotation with an exposure time of 1.5 s, and they were subsequently reconstructed.

3. Results and Discussion

3.1. The Microstructure of As-Cast Mg–10Zn–6.8Gd–4Y Alloy

Figure 1 shows the XRD results of the Mg–10Zn–6.8Gd–4Y alloy. The pattern suggests that the as-cast alloy was mainly composed of α -Mg and W phases, which is common in Mg–Zn–RE alloys [31]. The W phase has a face-centered cubic (FCC) structure and possesses high thermal stability [32].

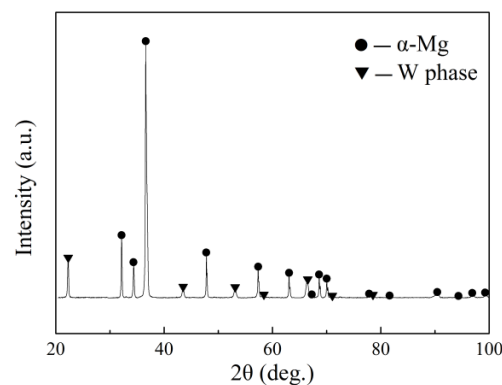


Figure 1. XRD pattern of the as-cast Mg–10Zn–6.8Gd–4Y alloy.

Figure 2 shows the SEM microstructure of the cast Mg–10Zn–6.8Gd–4Y alloy. The primary α -Mg grains exhibited a complex dendritic morphology and were surrounded by a eutectic phase network. The microstructure morphology suggests that the solidification mechanism of this alloy is dominated by dendrite growth. The eutectic microstructure seen in Figure 2a was enlarged for detailed examination and the result is shown in Figure 2b. It is seen that the eutectic microstructure is composed of gray microcrystalline and white phases having two morphologies (lamellar and block-shape structures), as shown by arrows in Figure 2b. It is pointed out that the eutectic structure was not continuous in some regions, as indicated by the dotted area in Figure 2b, indicating that there were differences in the grain orientation. TEM was carried out to further study the white eutectic phase in the Mg–10Zn–6.8Gd–4Y alloy, and the results are shown in Figure 3. A typical eutectic microstructure was observed, and the average lamellar distance was \sim 500 nm. The selected-area electron diffraction (SAED) patterns in Figure 3b,c suggest that the eutectic possesses both a hexagonal

closed-packed (HCP) structure (region b) and face-centered cubic (FCC) structure (region c). The EDS analysis in the TEM showed that the compositions of regions b and c were 99.5at.%Mg–0.5at.%Zn and 25.7at.%Mg–45.6at.%Zn–13.4at.%Y–15.3at.%Gd, respectively. This means the gray microstructure is eutectic Mg and the Zn/RE ratio (at.%) of the lamellar white eutectic phase was close to 1.5, suggesting that the white lamellar eutectic phase is the W phase. This is in accordance with the XRD results [33,34].

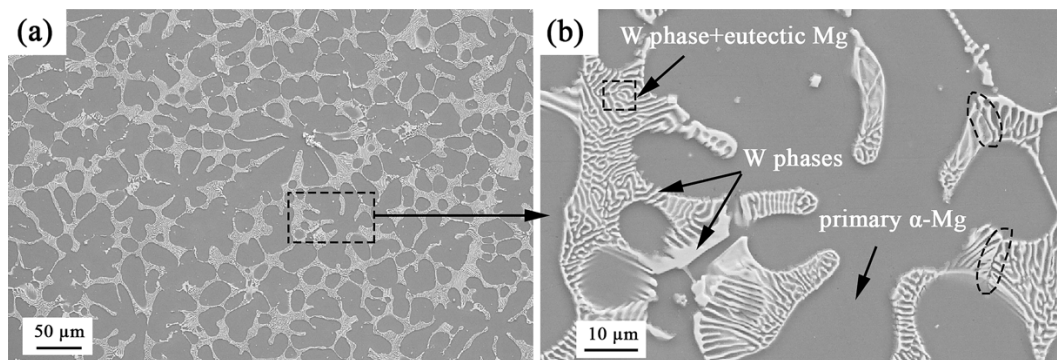


Figure 2. SEM microstructure of the as-cast Mg–10Zn–6.8Gd–4Y alloy: (a) low magnification; (b) high magnification.

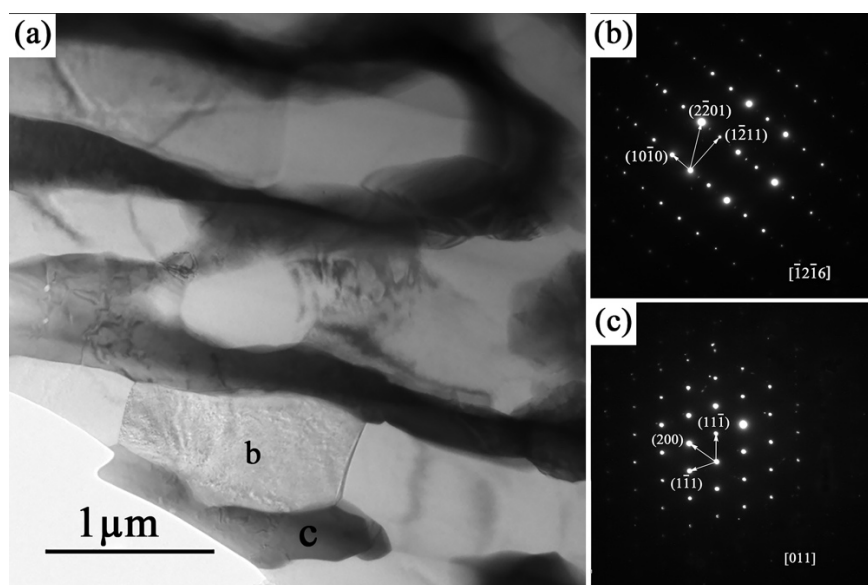


Figure 3. (a) TEM micrograph of the as-cast Mg–10Zn–6.8Gd–4Y alloy; (b,c) SAED patterns corresponding to regions b and c.

3.2. The Microstructures of Semi-Solid Mg–10Zn–6.8Gd–4Y Alloys

The solid fraction versus temperature curve of the Mg–10Zn–6.8Gd–4Y alloy was calculated to determine the holding temperature for semi-solid processing, and the results are shown in Figure 4. As shown in Figure 4, the solidus and liquidus temperatures of Mg–10Zn–6.8Gd–4Y were about 340 and 595 °C, respectively. The temperature of 580 °C was selected for the semi-solid coarsening experiments, corresponding to a solid fraction of 0.35.

In previous work on SSME, the main focus was on the microstructure evolution of the primary phases in magnesium alloys such as AS91, AZ91, and Mg–Gd alloys [7,15,17] during processing. The microstructures of these are mostly composed of a liquid matrix and primary α -Mg. With the prolongation of the isothermal holding time, the size of the primary α -Mg grains increased continuously and significantly without other changes in the microstructure. In this study, the changes in the

morphology and distribution of the secondary phase, as well as the formation of eutectic Mg grains, affected the microstructure of the alloys during the isothermal heat treatment.

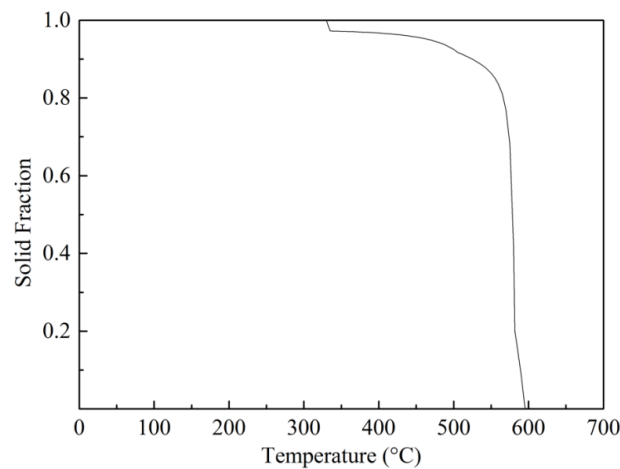


Figure 4. Solid fraction curve versus temperature of the Mg-10Zn-6.8Gd-4Y alloy.

Figure 5 shows the structural evolution of the semi-solid Mg-10Zn-6.8Gd-4Y alloy during isothermal holding at 580 °C for 2.5, 5, 10, 15, 30, 60, and 120 min. It was found that the dendrites in the cast samples were transformed into spheroids during the holding process. Although the original dendritic microstructures remained, the dendrite size became smaller than the as-cast ones, and the primary α -Mg grains tended to become gradually rounded after being held for 2.5 and 5 min, as shown in Figure 5a,b. The average grain size increased from ~ 30 μm to ~ 41 μm , and reached a peak value of ~ 41 μm after 5 min. Further extending the holding time to 10 min led to interior changes in the lamellar-shaped eutectic structure, and eutectic Mg grains with various morphologies appeared in the large eutectic regions, including polygon-, circular-, dendritic-shaped, etc., as shown in Figure 5c. At this stage, the presence of eutectic Mg reduced the overall average grain size to ~ 36 μm .

As shown in Figure 5d,e, when the holding time was prolonged, the eutectic Mg grains grew, and the adjacent small grains merged to form a large eutectic Mg grain. The average grain size increased, the grains became rounder and more regular, and the eutectic phases aggregated to form blocks after holding for 30 min. After isothermal heat treatment for 60 and 120 min, the eutectic Mg grains in the block-eutectic phases became rounder and were distributed more regularly. Some of them coalesced with adjacent large primary α -Mg grains. The size of the primary α -Mg grains became bulky, and the aforementioned aggregated eutectic areas basically disappeared, as shown in Figure 5f,g.

The 3D dendrites were segmented from the tomographic scans for further analysis. Figure 6 shows the 3D rendering of dendrites in Mg-10Zn-6.8Gd-4Y alloys after isothermal heat treatment from 0 to 120 min. Before the isothermal holding time reached 10 min, the dendrite arms gradually evolved into short and rounded ones. Meanwhile, the primary α -Mg grains began to grow and coarsen into spherical shapes in tandem with the increases in the isothermal holding time, as shown in Figure 6a–c. After holding for 10 min, the eutectic Mg grains began to appear in the eutectic regions. Owing to the obscurity of the boundary between the primary and eutectic Mg grains in the reconstructed images, the two kinds of grains were unavoidably connected in the 3D renderings, as shown in Figure 6e–h. When the holding time was prolonged, the eutectic Mg grains also grew, coarsened, and coalesced. The above 3D results are consistent with the SEM results. Figure 7 shows the 3D rendering of individual Mg grains in Mg-10Zn-6.8Gd-4Y alloys after isothermal heat treatment for 0, 5, 15, and 120 min. It can be clearly seen from Figure 7b that the dendrite tips became rounded, and the dendritic arms appeared shorter after being treated for 5 min, compared with that of the as-cast microstructure in Figure 7a. With the increase in holding time, the dendritic branches grew from the primary α -Mg grains due to

the coarsening process, as shown in Figure 7c,d. This observation further confirms the results observed in the 2D SEM microstructures.

Figure 8 shows the evolution of the average grain size of semi-solid Mg–10Zn–6.8Gd–4Y alloys. In the initial stage of isothermal processing (<10 min), the grains grew rapidly. After isothermal processing for 10 min, the average size of the grains started to decrease, because many new tiny and relatively equiaxial eutectic Mg grains started to appear in the eutectic structure, significantly increasing the number of grains in the alloy. It can be noticed in the figure that there was a slight increase in the grain size when the holding time increased from 15 to 30 min and from 60 to 120 min, while there was a slight decrease in the grain size when the holding time increased from 30 to 60 min. These fluctuations were mainly caused by the competition between the grain growth of large α -Mg dendrites by swallowing the surrounding eutectic Mg grains or liquid eutectic Mg and the changing number of eutectic Mg grains as they evolve. For example, because of the increase in the number of eutectic Mg grains over the holding time and their short coarsening period, the large number of fine eutectic Mg grains led to a sharp decrease in the average grain size from 30 to 60 min.

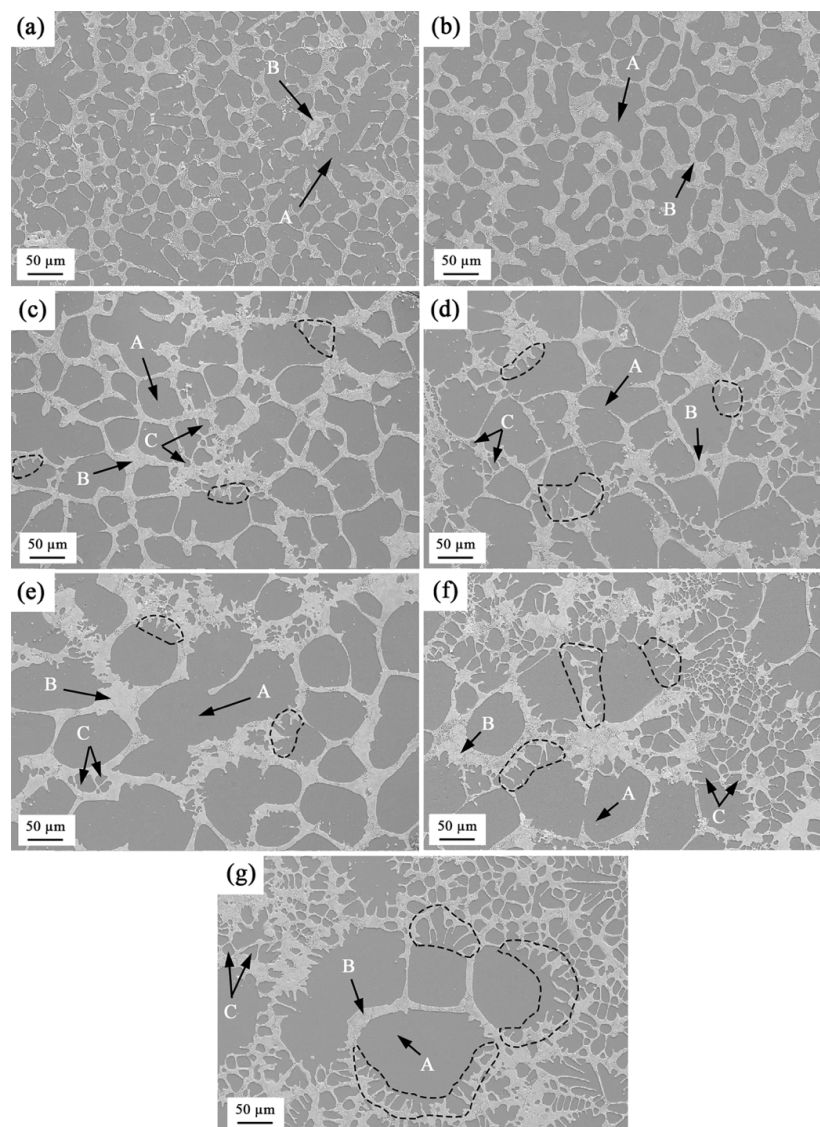


Figure 5. SEM microstructures of a semi-solid Mg–10Zn–6.8Gd–4Y alloy after an isothermal heat treatment at 580 °C for different holding times: (a) 2.5 min; (b) 5 min; (c) 10 min; (d) 15 min; (e) 30 min; (f) 60 min; (g) 120 min. A, B, and C indicate primary α -Mg grains, eutectic structures, and eutectic Mg grains, respectively.

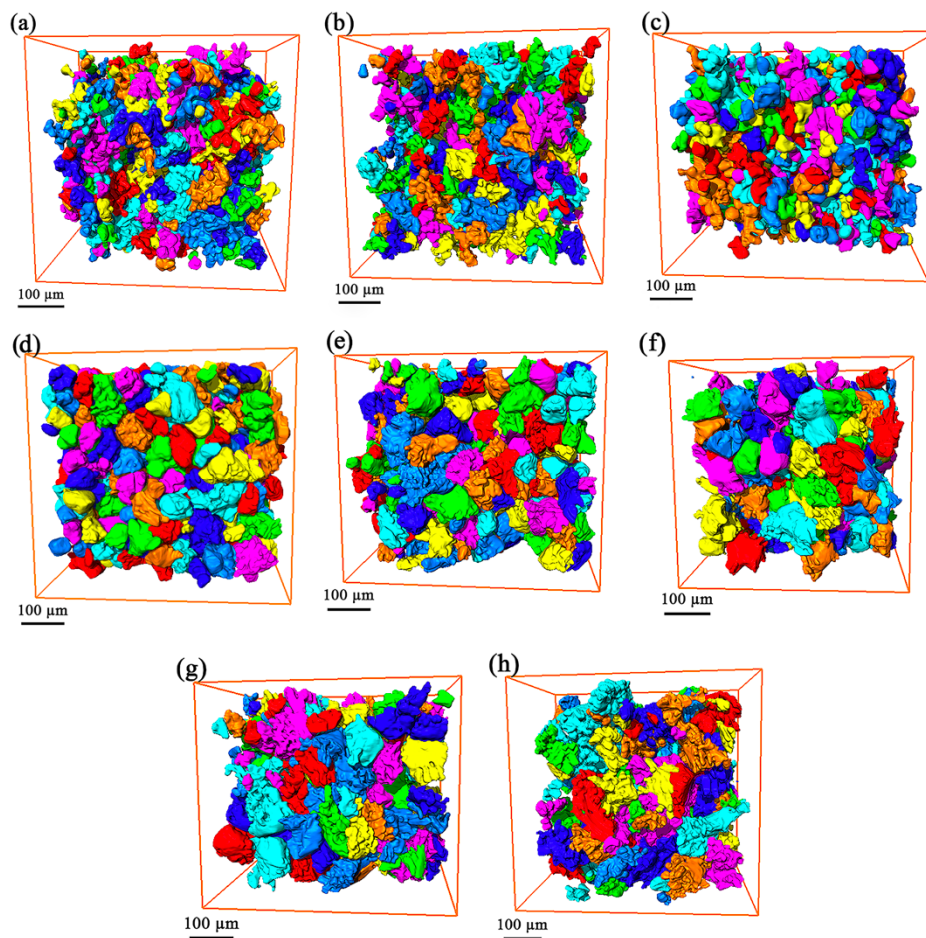


Figure 6. Three-dimensional rendering of Mg dendrites in Mg-10Zn-6.8Gd-4Y after an isothermal heat treatment at 580 °C for different holding times: (a) 0 min; (b) 2.5 min; (c) 5 min; (d) 10 min; (e) 15 min; (f) 30 min; (g) 60 min; (h) 120 min.

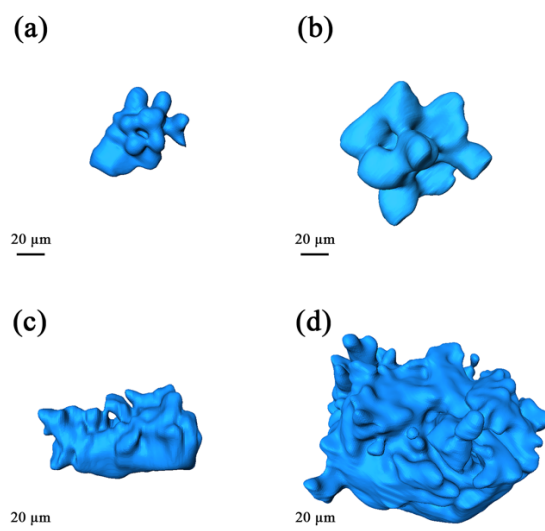


Figure 7. Three-dimensional rendering of an individual Mg grain in Mg-10Zn-6.8Gd-4Y after an isothermal heat treatment at 580 °C for different holding times: (a) 0 min; (b) 5 min; (c) 15 min; (d) 120 min.

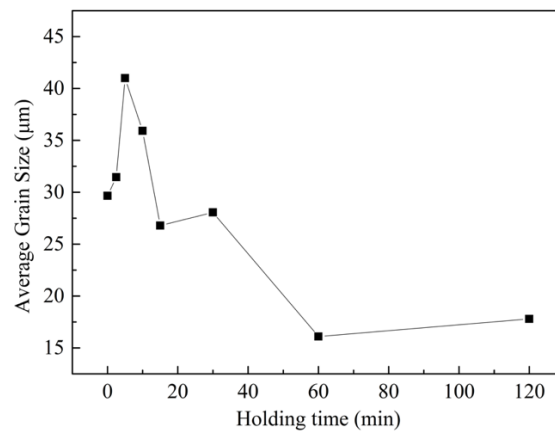


Figure 8. Effect of an isothermal heat treatment on the average grain size in Mg-10Zn-6.8Gd-4Y.

3.3. Coarsening Mechanism during Isothermal Heat Treatment

Electron probe microscope analysis (EPMA) was used to determine the element distribution, and the results are shown in Figure 9. There were two regions with high Mg concentration within the area scanned. The Zn, Y, and Gd contents were much higher in the eutectic structure than within the primary α -Mg grains. The line-scanning curve (Figure 9f) shows that when the eutectic Mg grains form, the Zn, Gd and Y elements in the center of a eutectic Mg grain would diffuse to the surrounding eutectic structures, leading to a decrease in the solute content in the area. This is especially obvious for the zinc content, which showed a large fluctuation and exceeded the magnesium content in a small region. One possible explanation for the above phenomenon during the isothermal heat treatment could be the Gibbs–Thomson effect. If the interface between the two phases is curved, a pressure difference occurs due to the interfacial tension [35]. The equilibrium solute supersaturation at the interface is proportional to the local mean curvature of the interface. The spatial variation of the equilibrium supersaturation at an interface with inhomogeneous curvature leads to a concentration gradient which excites the fluxes of enthalpy and solutes through the embedding matrix phase. These diffusion interactions stimulate the growth of flatter interface regions and lead to the remelting of more curved regions. The net effect of this process is that the average particle radius of the microstructures increases and the average curvature of the interfaces decreases correspondingly [36]. G.R. Ma et al. investigated the morphology changes of Mg_2Si phases in AS91 alloy during semi-solid isothermal heat treatment. According to the Gibbs–Thomson effect, the sites of the secondary phase Mg_2Si have a large curvature and high concentration of Si. Si atoms would diffuse to the flat interface where the concentration of Si is lower. This leads to dissolution at the positions with larger curvature. As a result, the Mg_2Si inclusions are modified [15]. An alloy element's concentration in the eutectic phase at large curvature can be expressed as [15,36,37]

$$C_{\alpha}(r) = C_{\alpha}(\infty) \exp\left(\frac{2\sigma v_B}{k_B T r}\right) \quad (1)$$

where $C_{\alpha}(r)$ is the alloy element's concentration at the site with a given curvature radius (r), $C_{\alpha}(\infty)$ is the alloy element's concentration at a flat interface, σ is the surface tension, v_B is the atomic volume of the alloy element, T is the temperature, and k_B is the shape coefficient. Therefore, a smaller curvature radius generally causes a higher concentration, and the different eutectic phase shapes cause different curvature radii, leading to a concentration gradient of the alloying elements. Therefore, the alloying atoms diffuse from an area where the curvature is larger, and the alloy-element concentration is higher, to a flat interface, with a lower alloy-element concentration. To recover the balance, the sharply curved regions of eutectic phases are dissolved.

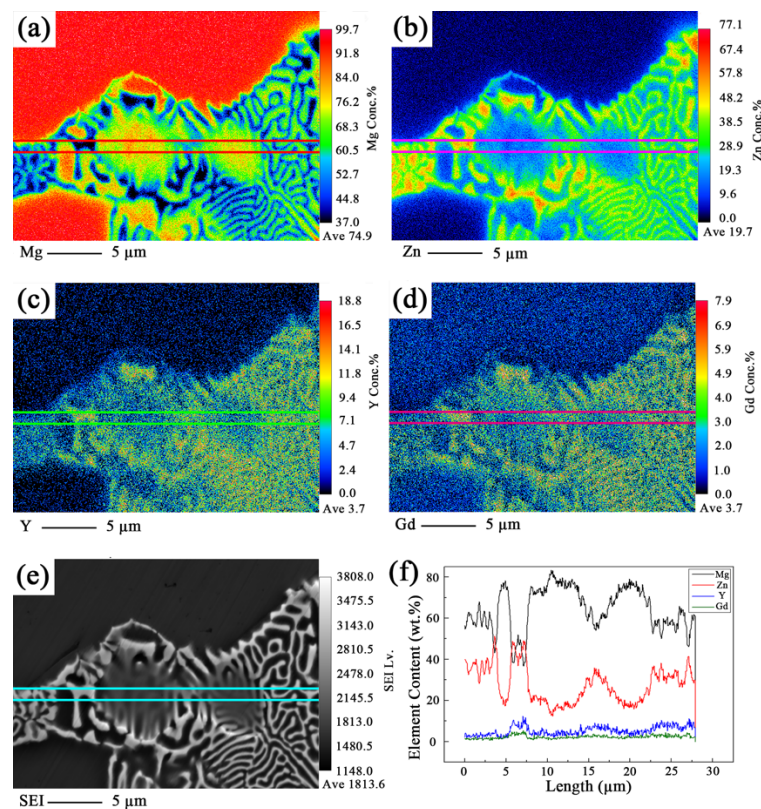


Figure 9. EPMA results of the Mg–10Zn–6.8Gd–4Y alloy after an isothermal heat treatment for 15 min: (a) Mg content distribution; (b) Zn content distribution; (c) Y content distribution; (d) Gd content distribution; (e) SEI image; (f) summary of element content distribution.

Previous studies have reported the impurity diffusion coefficients in HCP Mg alloys [38,39], and the diffusion coefficients of Mg and Zn are in the same order of magnitude, but are an order of magnitude higher than that of Gd and Y elements. This also explains why the Mg and Zn contents change greatly, while the contents of Gd and Y change slightly, as shown in Figure 9f. Some studies indicate that the diffusion of Mg atoms is faster than that of Y and Gd [38,40]. Due to the fact that the white eutectic structure is not completely closed, as shown in the dotted areas in Figure 2b, magnesium atoms could diffuse into the interior of the eutectic structure through the open channels during isothermal heat treatment and form secondary α -Mg grains. Owing to the long diffusion distance of magnesium atoms between the primary α -Mg and eutectic structure, the formation of the eutectic Mg grains is mainly due to the interdiffusion of magnesium atoms within the eutectic structure. Therefore, under these conditions, the average grain size variation curve presents the trend described in Figure 8.

There are two mechanisms believed to be responsible for the coarsening kinetics of the primary and eutectic Mg grains during the isothermal heat treatment, viz. grain coalescence and Ostwald ripening. The coarsening process is driven by the migration of grain boundaries at a high solid fraction, and the predominant mechanism is the coalescence of adjacent grains, which are remelting at the same time, so a balance exists between them. On the other hand, when the holding time increases, the Ostwald ripening mechanism dominates the coarsening process, in which the larger grains grow and the smaller ones dissolve, and predominantly big grains result. The driving force for this mechanism under isothermal heat treatment is a reduction of the interfacial free energy. After the composition becomes close to equilibrium, the interface size increases and becomes unstable, due to the presence of a large number of interfaces. To reduce the total interfacial energy, the grains will be coarsened by the aforementioned mechanism.

Finally, we summarize the phenomenon of microstructure coarsening, as observed in Mg–10Zn–6.8Gd–4Y. Figure 10 shows a schematic diagram of the microstructure evolution of

Mg–10Zn–6.8Gd–4Y alloys during isothermal heat treatment. The initial microstructure is composed of dendritic α -Mg and lamellar-shaped eutectic structure, as shown in Figures 10a and 2a. At the beginning, only the coarsening of primary α -Mg occurred (Figure 10a–c), as observed in other studies [17,41]. With increasing holding times, new, tiny eutectic Mg grains appeared inside the bulk eutectic phase and grew continually. Adjacent small eutectic Mg grains merged to form large ones or coalesced with the large primary α -Mg grains, as shown in Figure 10d–f. Meanwhile, the dendritic grain branches grew from the primary α -Mg grain boundaries after a period of isothermal heat treatment, as shown in the dotted areas in Figures 5c–g and 10d,e. There are two possible explanations for the appearance of the dendrite branches. One is that the eutectic Mg adjacent to the primary α -Mg grains diffuses into the primary grains, and they also coalesce over small areas, because of the small interstitial distance (~ 500 nm) and the unclosed channels, after isothermal heating for a period of time. The other possibility is that the already-formed eutectic Mg grains merge with the large primary α -Mg grains after a period of isothermal heat treatment. According to the experimental results and analysis, these two mechanisms, coalescence and Ostwald ripening, describe the grain coarsening during isothermal heat treatment.

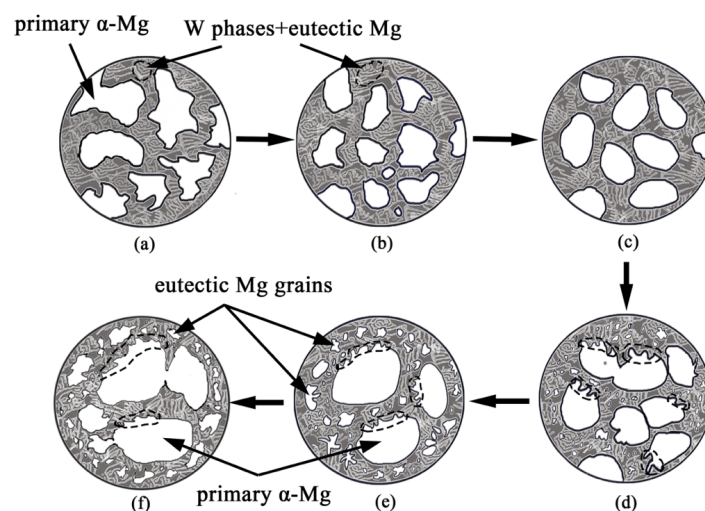


Figure 10. Schematic diagram of microstructure evolution in Mg–10Zn–4Y–6.8Gd during isothermal heat treatment: (a) as-cast microstructure; (b,c) microstructure evolution with only α -Mg grains growth; (d,e) microstructure evolution after appearance of eutectic Mg grains.

4. Conclusions

The effects of the holding time on microstructure evolution in Mg–10Zn–6.8Gd–4Y alloys during semi-solid isothermal heat treatment were investigated. According to the experimental results, the following conclusions can be obtained:

(1) The microstructure of cast and semi-solid Mg–10Zn–6.8Gd–4Y is mainly composed of α -Mg and eutectic structures (W phase + eutectic Mg). The eutectic structure is not completely closed in the 3D space, providing possible channels for the diffusion of magnesium atoms.

(2) With an increase in the isothermal holding time, the primary α -Mg grains gradually grow and coarsen. Fine eutectic Mg grains begin to appear in the eutectic structure after holding for 10 min, leading to a decrease in the overall grain size. The dendritic branches regrow in the primary α -Mg grains after holding for 10 min, due to the coarsening effects.

(3) During the isothermal heat treatment process of Mg–10Zn–6.8Gd–4Y, the grain coarsening is dominated by Ostwald ripening and coalescence.

Author Contributions: Conceptualization, S.N., Z.C. and E.G.; methodology, S.N., B.G. and X.W.; software, validation and formal analysis, S.N., Z.C. and E.G.; investigation, S.N., B.G., X.W., Z.C., E.G., and T.W.; writing—original draft preparation, S.N.; writing—review and editing, B.G., X.W., Z.C., E.G., and T.W.;

visualization, S.N., Z.C. and E.G.; supervision, project administration and funding acquisition, Z.C., E.G. and T.W.

Funding: This research was funded by the National Key Research and Development Program of China (Nos. 2016YFB0701203 and 2017YFA0403803), the National Natural Science Foundation of China (Nos. 51574058, 51771041, 51774065, 51671044), fundamental research funds for the central universities (Nos. DUT18RC(3)042).

Acknowledgments: The authors thank the National Key Research and Development Program of China (Nos. 2016YFB0701203 and 2017YFA0403803), the National Natural Science Foundation of China (Nos. 51574058, 51771041, 51774065, 51671044), fundamental research funds for the central universities (No. DUT18RC(3)042). The authors also thank the staff members of the BL13W1 beamline of Shanghai Synchrotron Radiation Facility (SSRF) for assistance in experiments.

Conflicts of Interest: The authors declare no conflict of interest.

References

1. Diem, W. Magnesium in different applications. *Auto Technol.* **2001**, *1*, 40–41.
2. Tekumalla, S.; Seetharaman, S.; Almajid, A.; Gupta, M. Mechanical properties of magnesium-rare earth alloy systems: a review. *Metals* **2015**, *5*, 1–39. [[CrossRef](#)]
3. Liu, H.; Ju, J.; Bai, J.; Sun, J.; Song, D.; Yan, J.; Jiang, J.; Ma, A. Preparation, microstructure evolutions and mechanical property of an ultra-fine grained Mg-10Gd-4Y-1.5Zn-0.5Zr alloy. *Metals* **2017**, *7*, 398. [[CrossRef](#)]
4. Tang, C.; Wu, K.; Liu, W.; Feng, D.; Wang, X.; Miao, G.; Yang, M.; Liu, X.; Li, Q. Effects of Gd, Y content on the microstructure and mechanical properties of Mg-Gd-Y-Nd-Zr alloy. *Metals* **2018**, *8*, 790. [[CrossRef](#)]
5. Zhang, J.; Tang, D.; Zhang, H.; Wang, L.; Wang, J.; Meng, J. Effect and application of rare earth element in magnesium alloys. *Chin. J. Rare Met.* **2008**, *32*, 659–667.
6. Rokhlin, L.L. *Magnesium Alloys Containing Rare Earth Metals: Structure and Properties*; Taylor & Francis: London, UK, 2003; pp. 32–45.
7. Su, G.; Cao, Z.; Liu, Y.; Wang, Y.; Zhang, L.; Cheng, L. Effects of semi-solid isothermal process parameters on microstructure of Mg-Gd alloy. *Trans. Nonferrous Met. Soc. Chin.* **2010**, *20*, s402–s406. [[CrossRef](#)]
8. Zheng, W.; Li, S.; Tang, B.; Zeng, D.; Guo, X. Effect of rare earths on hot cracking resistant property of Mg-Al alloys. *J. Rare Earths* **2006**, *24*, 346–351. [[CrossRef](#)]
9. Flemings, M.C. Behavior of metal-alloys in the semisolid state. *Metall. Trans. A* **1991**, *22*, 957–981. [[CrossRef](#)]
10. Ji, S.; Fan, Z.; Bevis, M.J. Semi-solid processing of engineering alloys by a twin-screw rheomoulding process. *Mater. Sci. Eng. A* **2001**, *299*, 210–217. [[CrossRef](#)]
11. Wang, W.; Jiang, B.; Yuan, S.; Jie, W.; Yang, G. Microstructure evolution during solidification of AZ91D magnesium alloy in semisolid. *J. Mater. Sci. Technol.* **2006**, *22*, 311–314.
12. Koren, Z.; Rosenson, H.; Gutman, E.M.; Unigovski, Y.B.; Eliezer, A. Development of semisolid casting for AZ91 and AM50 magnesium alloys. *J. Light Met.* **2002**, *2*, 81–87. [[CrossRef](#)]
13. Czerwinski, F. The generation of Mg–Al–Zn alloys by semisolid state mixing of particulate precursors. *Acta Mater.* **2004**, *52*, 5057–5069. [[CrossRef](#)]
14. Loué, W.R.; Suéry, M. Microstructural evolution during partial remelting of Al-Si7Mg alloys. *Mater. Sci. Eng. A* **1995**, *203*, 1–13. [[CrossRef](#)]
15. Ma, G.R.; Li, X.L.; Xiao, L.; Li, Q.F. Effect of holding temperature on microstructure of an AS91 alloy during semisolid isothermal heat treatment. *J. Alloys Compd.* **2010**, *496*, 577–581. [[CrossRef](#)]
16. Zhang, L.; Wu, G.; Cao, Z.; Ding, W. Effects of Ca content on the microstructure of semisolid Mg–13Al alloy produced via isothermal heat treatment. *J. Alloys Compd.* **2012**, *534*, 52–58. [[CrossRef](#)]
17. Nami, B.; Shabestari, S.G.; Miresmaeili, S.M.; Razavi, H.; Mirdamadi, S. The effect of rare earth elements on the kinetics of the isothermal coarsening of the globular solid phase in semisolid AZ91 alloy produced via SIMA process. *J. Alloys Compd.* **2010**, *489*, 570–575. [[CrossRef](#)]
18. Voorhees, P.W.; Glicksman, M.E. Ostwald ripening during liquid phase sintering—Effect of volume fraction on coarsening kinetics. *Metall. Trans. A* **1984**, *15*, 1081–1088. [[CrossRef](#)]
19. Masteghin, M.G.; Bertinotti, R.C.; Orlandi, M.O. Coalescence growth mechanism of inserted tin dioxide belts in polycrystalline SnO₂-based ceramics. *Mater. Charact.* **2018**, *142*, 289–294. [[CrossRef](#)]
20. German, R.M. Coarsening in sintering: grain shape distribution, grain size distribution, and grain growth kinetics in solid-pore systems. *Crit. Rev. Solid State Mater. Sci.* **2010**, *35*, 263–305. [[CrossRef](#)]

21. Chen, M.; Kattamis, T.Z. Dendrite coarsening during directional solidification of Al–Cu–Mn alloys. *Mater. Sci. Eng. A* **1998**, *247*, 239–247. [[CrossRef](#)]
22. Fife, J.L.; Voorhees, P.W. Self-similar microstructural evolution of dendritic solid–liquid mixtures during coarsening. *Scr. Mater.* **2009**, *60*, 839–842. [[CrossRef](#)]
23. Pompe, O.; Rettenmayr, M. Microstructural changes during quenching. *J. Cryst. Growth* **1998**, *192*, 300–306. [[CrossRef](#)]
24. Van Boggelen, J.W.K.; Eskin, D.G.; Katgerman, L. First stages of grain coarsening in semi-solid Al–Cu alloys. *Scr. Mater.* **2003**, *49*, 717–722. [[CrossRef](#)]
25. Chen, F.; Mao, F.; Chen, Z.; Han, J.; Yan, G.; Wang, T.; Cao, Z. Application of synchrotron radiation X-ray computed tomography to investigate the agglomerating behavior of TiB₂ particles in aluminum. *J. Alloys Compd.* **2015**, *622*, 831–836. [[CrossRef](#)]
26. Wang, M.Y.; Xu, Y.J.; Jing, T.; Peng, G.Y.; Fu, Y.N.; Chawla, N. Growth orientations and morphologies of α -Mg dendrites in Mg–Zn alloys. *Scr. Mater.* **2012**, *67*, 629–632. [[CrossRef](#)]
27. Maire, E.; Grenier, J.C.; Daniel, D.; Baldacci, A.; Klöcker, H.; Bigot, A. Quantitative 3D characterization of intermetallic phases in an Al–Mg industrial alloy by X-ray microtomography. *Scr. Mater.* **2006**, *55*, 123–126. [[CrossRef](#)]
28. Salvo, L.; Cloetens, P.; Maire, E.; Zabler, S.; Blandin, J.J.; Buffière, J.Y.; Ludwig, W.; Boller, E.; Bellet, D.; Josserond, C. X-ray micro-tomography an attractive characterisation technique in materials science. *Nucl. Instrum. Methods Phys. Res. Sect. B* **2003**, *200*, 273–286. [[CrossRef](#)]
29. Guo, E.; Phillion, A.B.; Cai, B.; Shuai, S.; Kazantsev, D.; Jing, T.; Lee, P.D. Dendritic evolution during coarsening of Mg–Zn alloys via 4D synchrotron tomography. *Acta Mater.* **2017**, *123*, 373–382. [[CrossRef](#)]
30. Shuai, S.; Guo, E.; Zheng, Q.; Wang, M.; Jing, T. Characterisation of three-dimensional dendritic morphology and orientation selection of α -Mg in Mg–Ca alloy using synchrotron X-ray tomography. *Mater. Charact.* **2016**, *111*, 170–176. [[CrossRef](#)]
31. Tahreen, N.; Zhang, D.F.; Pan, F.S.; Jiang, X.Q.; Li, D.Y.; Chen, D.L. Strengthening mechanisms in magnesium alloys containing ternary I, W and LPSO phases. *J. Mater. Sci. Technol.* **2018**, *34*, 1110–1118. [[CrossRef](#)]
32. Luo, S.; Pan, F.; Tang, A. Microstructure and mechanical properties at elevated temperature of Mg–Zn–Zr–Y alloy with W phase. *Hot Working Technol.* **2012**, *41*, 41–44. [[CrossRef](#)]
33. Jiang, H.S.; Qiao, X.G.; Zheng, M.Y.; Wu, K.; Xu, C.; Kamado, S. The partial substitution of Y with Gd on microstructures and mechanical properties of as-cast and as-extruded Mg–10Zn–6Y–0.5Zr alloy. *Mater. Charact.* **2018**, *135*, 96–103. [[CrossRef](#)]
34. Shi, F.; Wang, C.; Zhang, Z. Microstructures, corrosion and mechanical properties of as-cast Mg–Zn–Y–(Gd) alloys. *Trans. Nonferrous Met. Soc. China* **2015**, *25*, 2172–2180. [[CrossRef](#)]
35. Ratke, L.; Voorhees, P.W. *Growth and Coarsening: Ostwald Ripening in Material Processing*; Springer: Berlin, Germany, 2002; pp. 31–41.
36. Marsh, S.P.; Glicksman, M.E. Overview of Geometric Effects on Coarsening of Mushy Zones. *Metall. Mater. Trans. A* **1996**, *27*, 557–567. [[CrossRef](#)]
37. Nishioka, K.; Maksimov, I.L. Reconsideration of the concept of critical nucleus and the Gibbs–Thomson equation. *J. Cryst. Growth* **1996**, *163*, 1–7. [[CrossRef](#)]
38. Das, S.K.; Kang, Y.B.; Ha, T.; Jung, I.H. Thermodynamic modeling and diffusion kinetic experiments of binary Mg–Gd and Mg–Y systems. *Acta Mater.* **2014**, *71*, 164–175. [[CrossRef](#)]
39. Das, S.K.; Kim, Y.M.; Ha, T.K.; Jung, I.H. Investigation of anisotropic diffusion behavior of Zn in hcp Mg and interdiffusion coefficients of intermediate phases in the Mg–Zn system. *Calphad* **2013**, *42*, 51–58. [[CrossRef](#)]
40. Bermudez, K.; Brennan, S.; Sohn, Y.H. Intermetallic phase formation and growth in the Mg–Y System. In *Magnesium Technology 2012*; Mathaudhu, S.N., Sillekens, W.H., Neelameggham, N.R., Hort, N., Eds.; Springer International Publishing: Berlin, Germany, 2016; pp. 145–148.
41. Liu, W.; Yang, D.D.; Quan, G.F.; Zhang, Y.B.; Yao, D.D. Microstructure evolution of semisolid Mg–2Zn–0.5Y alloy during isothermal heat treatment. *Rare Met. Mater. Eng.* **2016**, *45*, 1967–1972.

